

Article

FACEs: A deep learning-based parametric model to improve rosacea diagnoses

Seungman Park ^{1,*}, Anna L. Chien ², Beiyu Lin ³, and Keva Li ⁴

¹ Department of Mechanical Engineering, University of Nevada, Las Vegas, Las Vegas, NV 89154, USA; seungman.park@unlv.edu

² Department of Dermatology, Johns Hopkins University School of Medicine, Baltimore, MD 21287, USA; achien3@jhmi.edu

³ Department of Computer Science, University of Nevada, Las Vegas, Las Vegas, NV 89154, USA; beiyu.lin@unlv.edu

⁴ Molecular and Cellular Biology, Johns Hopkins University, Baltimore, MD 21218, USA; kevali625@gmail.com

* Correspondence: seungman.park@unlv.edu

Featured Application: The proposed workflow for the classification of rosacea can be utilized for other types of skin diseases to improve classification performance.

Abstract: Rosacea is a chronic inflammatory skin disorder that causes visible blood vessels and redness on the nose, chin, cheeks, and forehead. However, visual assessment, the current standard method used to identify rosacea, is often subjective among clinicians and results in high variation. Recent advances in artificial intelligence have allowed for the effective detection of various skin diseases with high accuracy and consistency. In this study, we develop a new methodology, coined “five accurate CNNs-based evaluation system (FACEs),” to identify and classify rosacea more efficiently. First, 19 CNN-based models that have been widely used for image classification were trained and tested via training and validation data sets. Next, 5 best performance models were selected based on accuracy, which served as a weight value for FACEs. At the same time, we also applied a majority rule to 5 selected models to detect rosacea. Results exhibited that the performance of FACEs was superior to that of 5 individual CNN-based models and the majority rule in terms of accuracy, sensitivity, specificity, and precision. In particular, the accuracy and sensitivity of FACEs were highest, and specificity and precision were higher than most of the individual models. To improve the performance of our system, future studies must consider patient details, such as age, gender, and race, and perform comparison tests between our model system and clinicians.

Citation: To be added by editorial staff during production.

Academic Editor: Firstname Lastname

Received: date

Accepted: date

Published: date

Publisher's Note: MDPI stays neutral with regard to jurisdictional claims in published maps and institutional affiliations.



Copyright: © 2022 by the authors. Submitted for possible open access publication under the terms and conditions of the Creative Commons Attribution (CC BY) license (<https://creativecommons.org/licenses/by/4.0/>).

1. Introduction

Rosacea is a chronic inflammatory skin disorder that causes visible blood vessels and redness on the human face [1], a condition that affects more than 16 million Americans [2]. Globally, the prevalence of this skin condition is thought to range from 0.2% to 22% of the population in North America and Europe [3,4]. Rosacea is categorized into 4 types: erythematotelangiectatic, papulopustular, phymatous, and ocular rosacea [5,6]. However, it is often difficult to distinguish one type from another [7]. In addition, visual assessment of rosacea, the standard clinical diagnostic method, is often subjective among clinicians and results in high variation [8–10]. As such, in many cases, rosacea is misdiagnosed as other skin disorders, such as acne, eczema, and lupus, or vice versa due to their similarities in appearance [11].

Over the past decade, advances in computer-aided diagnosis and treatment using artificial intelligence have allowed for the detection of various skin diseases with high accuracy and consistency [12]. Furthermore, due to the COVID-19 pandemic and self-isolation in patients, telemedicine, which doesn't require direct contact between clinicians and patients, has gained popularity [13]. The skin diseases for deep learning-based classification are diverse, ranging from cancer to acne, eczema, psoriasis, etc. However, the majority of the studies have been focused on skin cancer research. [14–22]. Hosny et al. employed a pre-trained deep learning network such as AlexNet to classify three different lesions (melanoma, common nevus, and atypical nevus) [23]. El-Khatib et al. developed a new effective decision system to distinguish melanoma from a nevus, which combines several deep learning and machine learning models [24]. They employed 5 well-known convolution neural network (CNN) models to develop a global classifier, which is the methodology used in this study, but they did not investigate numerous CNN models to find the 5 best. Moreover, they only tested a linear function to calculate the global index of decision and only tested the evaluation factor value (i.e., $\alpha=0.7$). Thomas et al. developed a new deep-learning method for the effective detection of non-melanoma skin cancers, which are the most common skin cancers: basal cell carcinoma (BCC), squamous cell carcinoma (SCC), and intraepidermal carcinoma (IEC). Codella et al. used both deep learning and machine learning models to detect diverse skin lesions, including melanoma [25]. This study utilized the International Skin Imaging Collaboration (ISIC) database to classify 2624 dermoscopic images based on a sparse coding, deep residual network, and support vector machine. Results displayed high performance values of classification with 93.1% accuracy, 92.8% specificity, and 94.9% sensitivity.

In addition to cancer, some efforts have been made to classify non-cancerous skin diseases through artificial intelligence, including psoriasis, atopic dermatitis, eczema, acne, hemangioma, onychomycosis, and so on [8,26,27]. Ramli et al. employed a k-means clustering to classify acne lesions by collecting acne samples with different grades (mild, moderate, severe, and very severe) from 98 patients [28]. Aggarwal et al. trained TensorFlow Inception version-3 to recognize 5 dermatological diseases, including atopic dermatitis, acne, psoriasis, impetigo and rosacea [29]. They measured 6 statistical parameters such as sensitivity, specificity, PPV, NPN, MCC, and F1 score, with the application of data augmentation. Thomsen et al. adopted a pre-trained deep model, VGG-16, for the classification of multiple skin diseases (acne, rosacea, psoriasis, eczema, and cutaneous t-cell lymphoma) [15]. Goceri tested the performance of several deep learning models (U-Net, InceptionV3, ResNet, InceptionResNetV2, and VGGNet) to classify 5 common skin disorders: acne vulgaris, hemangioma, psoriasis, rosacea, and seborrheic dermatitis. The study showed that the ResNet152 produces the highest accuracy [26].

Motivated by the recent success of artificial intelligence in detecting diverse skin disorders and diseases from clinical photos, we present a novel methodology integrating the existing CNN-based deep learning models to detect rosacea effectively. A total of 19 CNN-based models specialized in image classification were utilized and trained to recognize patterns from patients' clinical images. The top 5 models were then selected in terms of accuracy, and subsequently, their accuracy values were used as weights for our generalized global model, coined "five accurate CNNs-based evaluation system (FACES)." Using the 5 chosen models, we also applied a majority rule to classify rosacea, and its performance was compared with individual CNNs and FACES.

The material and methods section addresses the detailed methodology of FACES using different functions. Next, in the results section, we present the performance values for current and individual CNN models using 4 parameters. Finally, we discuss the potential limitations and future works in the discussion and conclusions sections.

2. Related Work

Currently, extremely few studies have been performed on the automated identification only targeting rosacea using a deep learning or machine learning model, compared to other skin disorders. In addition, even though there are some studies, they usually include other skin lesions (**Table 1**), as mentioned above, rather than targeting rosacea alone, which can cause poor performance in terms of accuracy [26]. Recently, Binol et al. developed a new deep learning model, Ros-NET, to detect rosacea lesions by combining information from varying image scales and resolutions [14,30]. They estimated the Dice coefficient and false positive rate as a global measure using Ros-Net, whose results were compared with two well-known pre-trained deep learning models: Inception-ResNet-v2 and ResNet-101. However, most of these studies selected only a few models and compared their accuracy values to provide the best performance model. In this way, we could neglect the possibility that a better model might exist elsewhere. Hence, it is essential to develop a generalized global model encompassing numerous existing high-performance models.

Table 1. Previous related studies for the indentificatin of rosacea

Method	Skin Lesions	References
U-Net, VGGNet, Inception-v3, InceptionResNet-v2, and ResNet	rosacea, acne vulgaris, hemangioma, psoriasis, and seborrheic dermatitis	Goceri [26]
Inception-v3	rosacea, acne, atopic dermatitis, psoriasis, and impetigo	Aggarwal [29]
DenseNet201	rosacea, acne vulgaris, hemangioma, psoriasis, and seborrheic dermatitis	Goceri [31]
VGG-16	rosacea, acne, psoriasis, eczema, and cutaneous t-cell lymphoma	Thomsen et al. [15]
Ros-Net	rosacea	Binol et al. [14]
Inception-ResNet-v2	rosacea	Binol et al. [30]

3. Materials and Methods

3.1. Methodology for skin rosacea detection combining the 5 best classifiers

The clinical images were obtained from 40 patients with rosacea and 59 control groups from Johns Hopkins University Hospital (**Figs. 1a-b**). In order to improve the rosacea classification performance, we used multi-view clinical photos, which are photos of the same patient from different views. The high performance of multi-view, multi-modal, and integration approaches in machine learning and deep learning for image classification have been reported previously [32,33]. The images in the region of interest were segmented with different shapes and sizes, and subsequently, the segmented images were augmented by rotating and scaling (**Fig. 1a**). The augmentation options include random reflections based on the x-axis (i.e., horizontal flipping), random rotation within the rate [-90, 90], and random rescaling within the range [1, 2]. The resolution of the images is approximately 15-20 pixels/mm. A total of 600 images (66% of the entire data set) for each group were used for training through the well-known 19 pre-trained CNNs (**Fig. 1c**). A total of 200 images (22%) for each group were utilized for validation, and 110 images (12%) were utilized as test images. After training the CNN-based models, all models were tested

to classify images using the validation data set. Consequently, the top 5 CNN-based models were selected based on accuracy to apply them to FACES (Fig. 1c) as follows: ResNet-101 [34] (accuracy: 90.75%), DarkNet-19 [35] (90.25%), DarkNet-53 [36] (89.5%), ResNet-50 [37] (89.0%), and GoogleNet [38] (88.5%) (**Table 2**).
 133
 134
 135
 136
 137
 138

Table 2. Properties of the 5 used models for FACES

Network	Depth	Size	Parameters (Millions)	Image Input Size
ResNet-101	101	167 MB	44.6	224 by 224
DarkNet-19	19	78 MB	20.8	256 by 256
DarkNet-53	53	155 MB	41.6	256 by 256
ResNet-50	50	96 MB	25.6	224 by 224
GoogleNet	22	27 MB	7.0	224 by 224

Since all of the selected 5 methods are CNN models that take a linear O(n) time, where n is the number of input pixels [39]. Floating point operations per second (FLOPS) reflects the computation complexity of CNN models. The FLOPs for ResNet101, ResNet50, DarkNet53, DarkNet19, and GoogleNet are 7.6, 3.8, 53.6, 5.58, and 1.5 (billion), respectively. For our linear model, the total FLOPs are the summation of FLOPs of each selected method (i.e., $7.6+3.8+53.6+5.58+1.5 = 72.08$ billion) because our methods are feedforward, traveling forward through the entire network.
 139
 140
 141
 142
 143
 144
 145
 146

Stochastic gradient descent with a momentum (SGDM) optimizer was used as a solver. Different values of initial learning rate (0.0001-0.01), validation frequency (1-10), max epochs (5-50), and mini-batch sizes (3-30) were tested to find optimum values for the highest accuracy because different CNN models exhibited different optimized values. In addition, L2 regularization was applied with a value of 0.0001 as another hyperparameter. The training time was highly dependent on the types and depths/layers of models ranging from 10 minutes to 7 hours. All CNN models and FACES were run on a single CPU (Intel(R) Core(TM) i5-8265U CPU @ 1.80GHz) and 8.00 GB RAM.
 147
 148
 149
 150
 151
 152
 153
 154

The accuracy values from the top 5 CNN-based models were used as weights in the the FACES with the functions of 1st, 2nd, 3rd, and 4th degrees as follows:
 155
 156
 157

$$W = \sum_{i=1}^5 w_i^n d_i \quad (1)$$

$$W \geq \alpha W_{max} \text{ and } W_{max} = \sum_{i=1}^5 w_i^n \quad (2)$$

where n is 1, 2, 3, or 4 for linear, quadratic, cubic, and biquadratic functions, respectively; W is the FACES index of decision; w_i is the weight (i.e., accuracy calculated in the validation phase for each classifier); d_i is the individual decision where 1, if the classifier, indicates rosacea; otherwise, 0, and α is the evaluation factor whose optimized value is determined using a parametric study testing α ranging from 0.1 to 0.9 with an increase of 0.1. It should be noted that FACES detects rosacea if threshold condition (2) is satisfied.
 160
 161
 162
 163
 164
 165
 166
 167

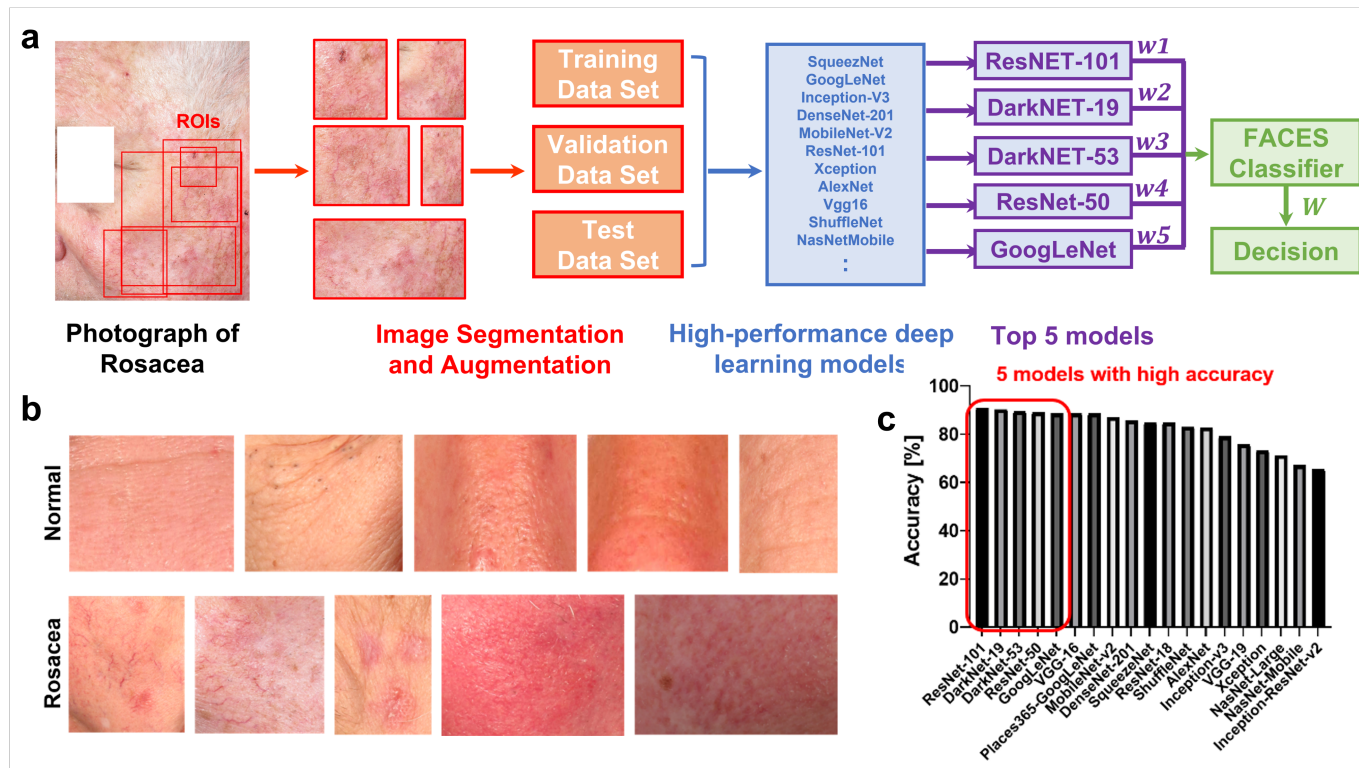


Figure 1. A five accurate CNNs-based evaluation system (FACES). **a.** The workflow of FACES for identifying rosacea lesions. **b.** Example images of normal and rosacea skin. **c.** Accuracy values from 19 pre-trained CNNs

3.2. Methodology for skin rosacea detection using the majority rule

In addition to FACES, using the top 5 CNN-based models, the majority rule was applied to classify rosacea. In brief, among 5 selected CNN-based models, if the number of models indicating rosacea is equal to or greater than 3, the decision by the majority rule denotes rosacea. Otherwise, it indicates normal skin. All deep learning models used in this study were implemented using MATLAB R2021b.

3.3. Analysis of 4 performance parameters

The accuracy, sensitivity, specificity, and precision of each model were calculated based on the confusion matrix containing true negative (TN), false negative (FN), true positive (TP), and false positive (FP) (Fig. 2 and Table 3) to evaluate performance.

		Predicted Class	
		Negative	Positive
True Class	Negative	True Negative (TN)	False Positive (FP)
	Positive	False Negative (FN)	True Positive (TP)

Figure 2. Schematic representation of the confusion matrix

Table 3. Parameters of performance used in this study

Performance parameter	Formula
Accuracy	$(TN+TP)/(TN+FP+FN+TP)$

Sensitivity	TP/(TP+FN)
Specificity	TN/(TN+FP)
Precision	TP/(FP+TP)

188

4. Results

We tested the effects of α ranging from 0.1 to 0.9 on the rosacea classification in the linear, quadratic, cubic, and biquadratic functions, respectively. The confusion matrices with respect to α are shown in **Figs 3–6**. For the linear function, the confusion matrix showed that true negative (TN) and false negative (FN) tend to increase as the evaluation factor increases, while true positive (TP) and false positive (FP) decrease (**Fig. 3**). At the confusion matrix of highest accuracy (92.27%, $\alpha=0.4$), 10% (11/110) of rosacea and 5.45% (6/110) of normal skin are misinterpreted as normal skin and rosacea, respectively.

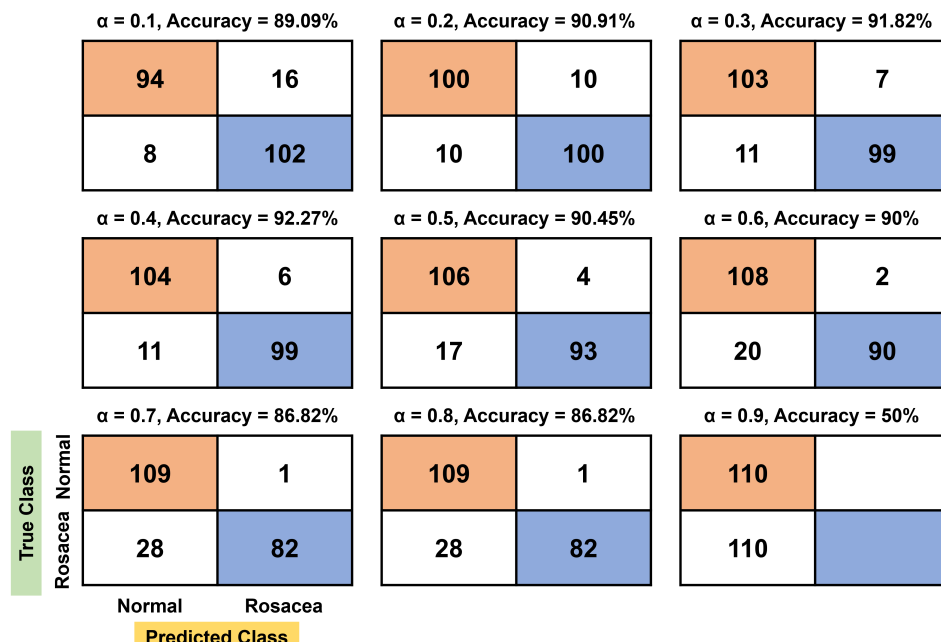
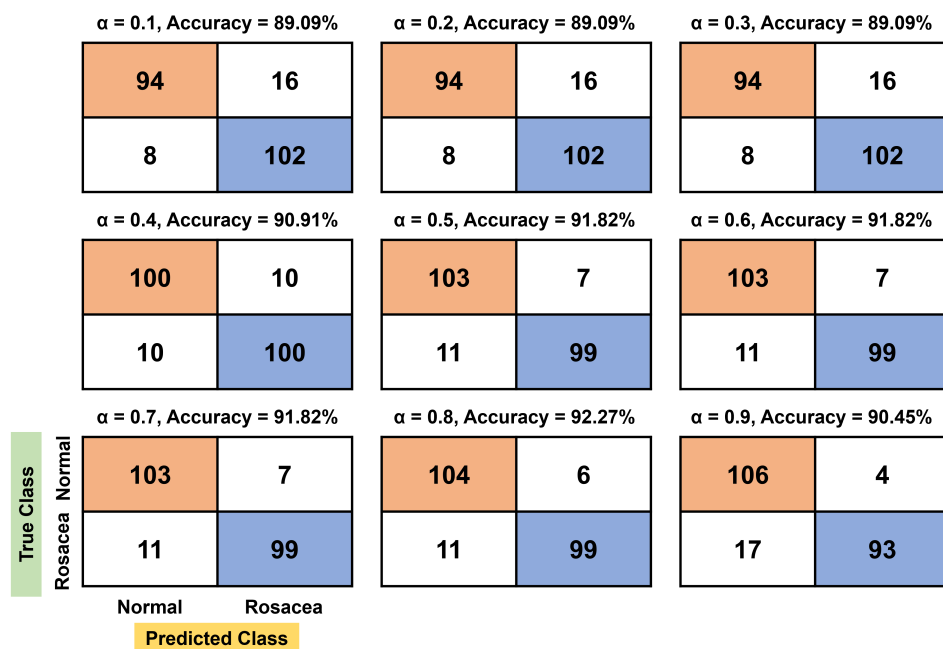
189
190
191
192
193
194
195
196
197

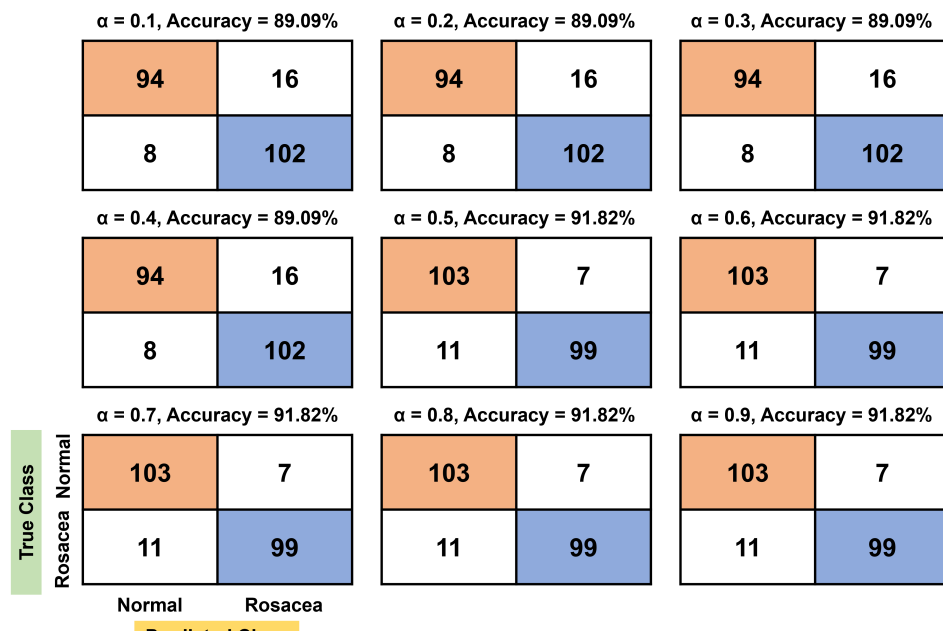
Figure 3. Confusion matrix and accuracy with respect to α for the linear function

For the quadratic function, there are two stagnant areas showing constant TN, FN, TP, and FP: 0.1 – 0.3 and 0.5 – 0.7 (**Fig. 4**). The best accuracy (92.27%) value is found to be at 0.8 of α where 10% (11/110) of rosacea and 5.45% (6/110) of normal skin are misclassified as normal skin and rosacea, respectively. Overall, TN and FN tend to increase more gradually with the increasing evaluation factor compared to the linear function, while TP and FP tend to decrease.

198
199
200
201
202
203
204
205
206
207

Figure 4. Confusion matrix and accuracy with respect to α for the quadratic function

For the cubic function, there are two large stagnant regions: the first region ranging 0.1 to 0.4 and the second region ranging from 0.5 to 0.9 (Fig. 5). The confusion matrix showed constant accuracy for each of the first and second stagnant areas as 89.09% and 92.27%, respectively. It should be noted that TP of the first region is higher than that of the second region, while TN is the opposite, showing a lower value in the first region. At the region of highest accuracy (91.82%), 10% (11/110) of rosacea and 6.36% (7/110) of normal skin are misinterpreted as normal skin and rosacea, respectively.

Figure 5. Confusion matrix and accuracy with respect to α for the cubic function

For the biquadratic function, a single α (0.5) shows the best accuracy (92.27%), while two stagnant regions (0.1–0.4 and 0.6–0.9) reveal accuracy values as 89.09% and 91.82%, respectively (Fig. 6). At the confusion matrix of highest accuracy (92.27%, $\alpha=0.5$), 9.09%

(10/110) of rosacea and 5.45% (6/110) of normal skin are misinterpreted as normal skin and rosacea, respectively.

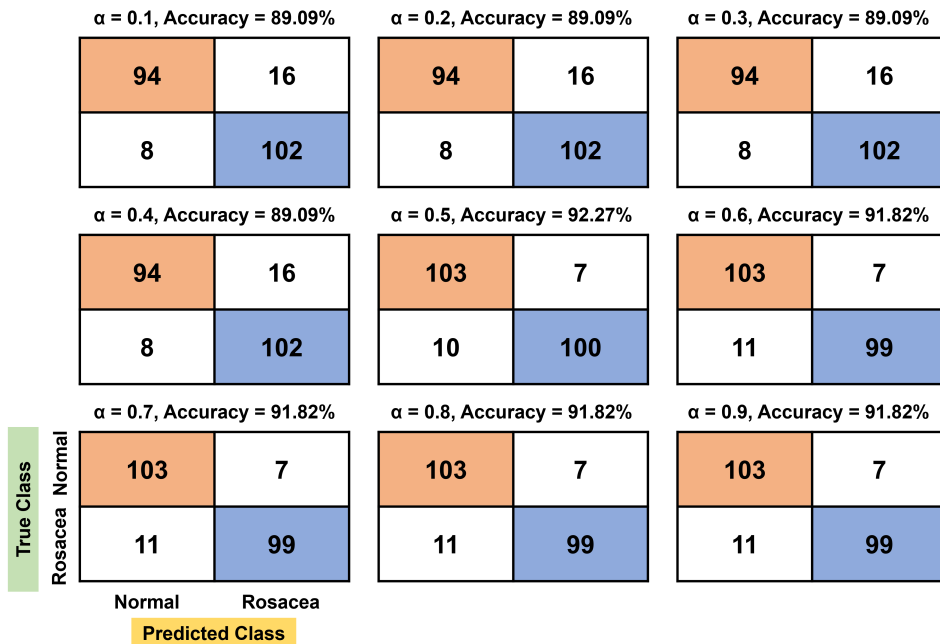


Figure 6. Confusion matrix and accuracy with respect to α for the biquadratic function

The confusion matrix created by the majority rule yields 90.45% accuracy as well as TN (106), which are the second largest, following ResNet-101 (91.36% for accuracy and 107 for TN) (**Fig. 7**). In addition, in the majority rule, 15.45% (17/110) of rosacea and 3.64% (4/110) of normal skin are misinterpreted as normal skin and rosacea, respectively.

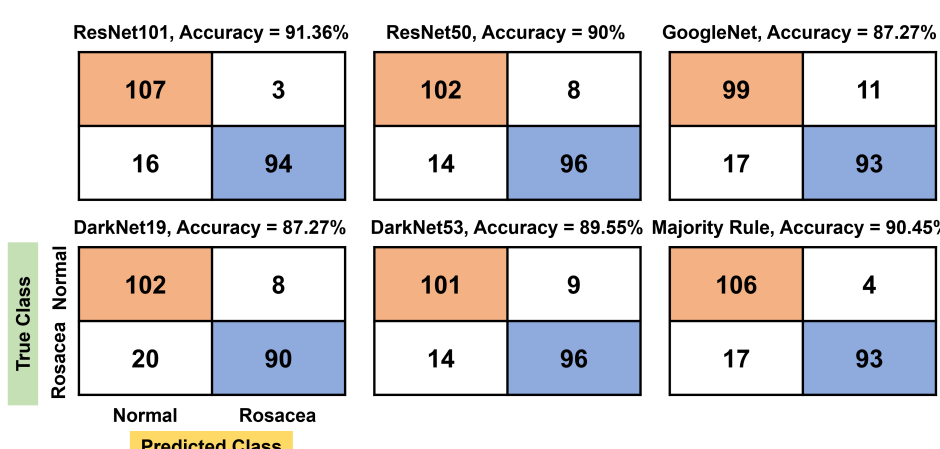


Figure 7. Confusion matrix and accuracy by the majority rule and other individual CNN models

Based on the results from the confusion matrices, accuracy is shown as a function of α for each function. Results showed that there is a significant impact of the evaluation factor on the accuracy, but their distribution depends highly on the degree of function (**Fig. 8a**). To be more specific, for the linear function ($n=1$), accuracy tends to increase up to 0.4 of α continually, but decreases after that. For the quadratic, cubic, and biquadratic functions ($n=2, 3$, and 4), the accuracy drastically increases at 0.3 or 0.4 of α and remains almost constant after 0.5 of α . The average accuracy values are 0.853, 0.907, 0.906, and 0.906 for the linear, quadratic, cubic and biquadratic functions, respectively. The highest accuracy is 92.27% ($\alpha=0.4$), 92.27% ($\alpha=0.8$), 91.82% ($\alpha \geq 0.5$), and 92.27% ($\alpha=0.5$) for the

linear, quadratic, cubic and biquadratic functions, respectively. When both the highest and average accuracy are considered, the quadratic function can be selected as the best performance function. Noticeably, all 4 performance parameters driven by FACES are at least greater than or equal to 0.9, while those by other models are not.

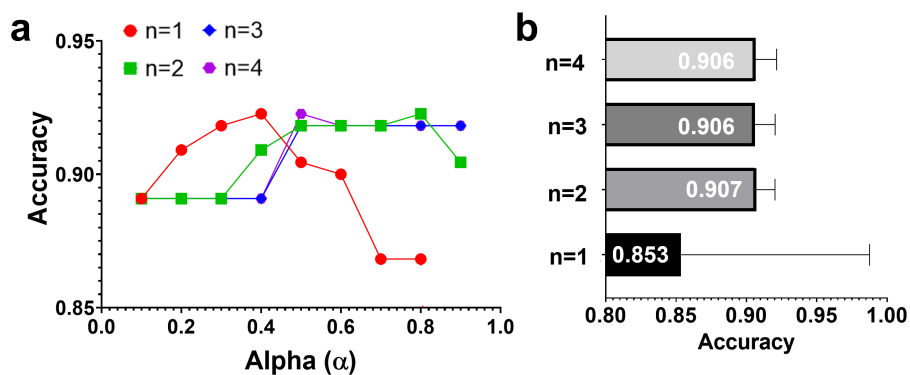


Figure 8. Parametric analysis in different functions with respect to the evaluation factor (α) of the FACES. **a.** Effects of α on accuracy values with different degrees of polynomial order (n) **b.** Average accuracy values of each function: linear (n=1), quadratic (n=2), cubic (n=3), and biquadratic (n=4) functions

We compared the performance of the FACES with that of individual CNN-based models and the majority rule. Results showed that FACES displays the best performance, revealing the highest accuracy (92.27%), followed by ResNet-101 (91.36%) and Majority Rule (90.45%) (Fig. 9a) as well as the highest sensitivity (0.90), followed by ResNet50 (0.873) and DarkNet53 (0.873) (Fig. 9b). However, FACES's specificity (0.945) and precision (0.943) are the third highest, following ResNet101 (0.973 for specificity and 0.969 for precision) and Majority Rule (0.964 and 0.959).

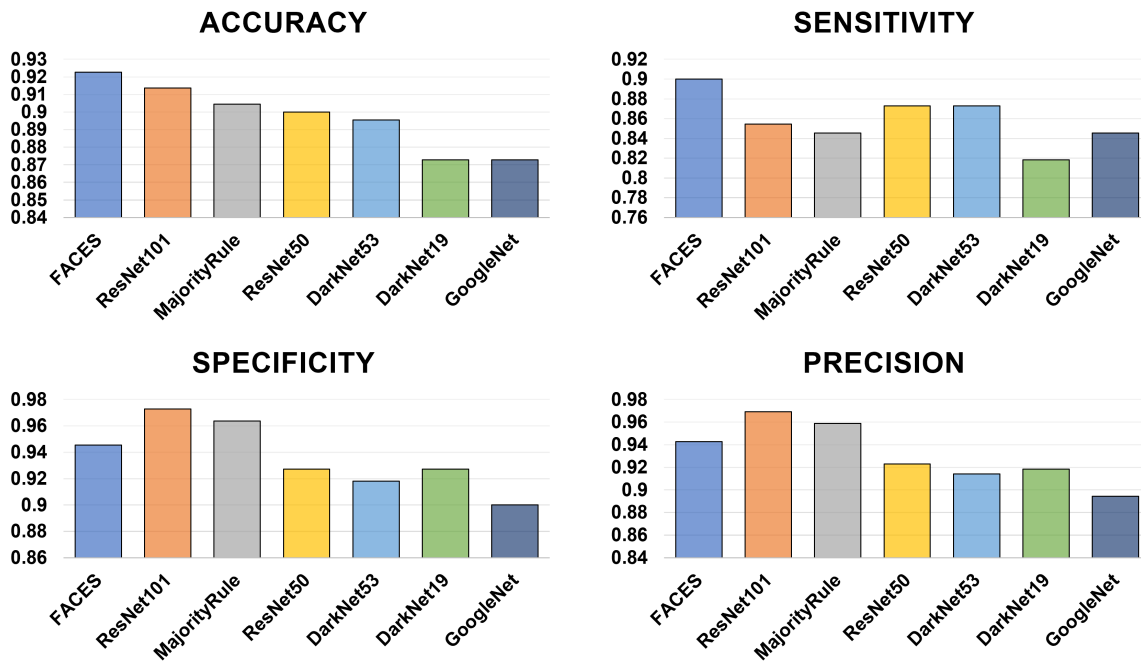


Figure 9. Comparison of performance of the FACES with that of individual CNNs and the majority rule in the testing phase

5. Discussion

Different individual CNN models have different performances for image classification and identification. In this study, by combining the results of these models, we developed a better system with higher accuracy to detect rosacea. A comparison between the

results of our proposed system and the results produced by other studies is shown in **Table 4**. Our proposed system shows better performance (92.27%) than that of the study with the highest accuracy (90.2%, Ros-Net).

Table 4. Comparison of accuracy values for the rosacea detection

Method	Accuracy	References
FACES	92.27%	Current study
ResNet-50	79%	[26]
Ros-Net		
• Overlapping image patches	90.2%	[14,30]
• Non-overlapping image patches	88%	
DenseNet201	87.81%	[31]
VGG-16	88.64%	[15]

For the rosacea identification and classification, we utilized clinical photos taken by a digital camera covering the whole face. However, a single photo might not cover the proportion of the skin lesion, thereby hardly representing or even distorting the features of rosacea. To overcome such limitations, we took photos from at least 3 different angles (i.e., multi-view learning), which contain the whole lesion of rosacea. Moreover, clinical photos were segmented and augmented to integrate different-scaled images to provide both microscopic and macroscopic characteristics of rosacea to improve the performance of FACES.

There are still limitations to be addressed and factors to be explored in the future to improve FACES's ability to detect rosacea. First, we did not compare the performance between FACES and experienced dermatologists to validate our method. Hence, comparison tests are required to warrant using our detection tool in clinical settings. In addition, we did not consider several important parameters, such as race, age, or gender, which can be highly associated with the occurrence of rosacea, thus affecting FACES's classification abilities. Early studies demonstrated that rosacea is an age-related disease that occurs more frequently at an older age, particularly above the age of 65 years [40,41]. Moreover, women under the age of 49 were found to be more affected by rosacea, while rosacea was more prevalent in men over 50 [40]. Rosacea's prevalence is also highly dependent on race. Prior research illustrated that Hispanics and Latinos are more susceptible to rosacea compared to African Americans or Asians [42]. Taken together, these limitations, as well as factors such as age, gender, or race, should be considered in future studies to enhance the performance of artificial intelligence. Such an approach will shed light on the new effective diagnoses and rosacea treatment in clinical practice.

6. Conclusions

In this study, we develop a new decision system based on high-performance CNN-based pre-trained models for the detection of rosacea, FACES. FACES outperforms other individual models, showing greater accuracy and sensitivity than each individual classifier. In addition, FACES performs well in terms of specificity and precision. It is expected that the current workflow can be extended and applied to other types of skin diseases in future studies. However, diverse rosacea-related factors need to be systematically considered as a deep learning parameter in future studies to improve rosacea identification.

Abbreviation

FACES: five accurate CNNs-based evaluation system
BCC: basal cell carcinoma

SCC: squamous cell carcinoma	313
IEC: intraepidermal carcinoma	314
TN: true negative	315
FN: false negative	316
TP: true positive	317
FP: false positive	318
Author Contributions: Conceptualization, S.P. and A.C.; methodology, S.P.; validation, S.P. and B.L.; formal analysis, S.P. and K.L.; investigation, S.P. and K.L.; resources, A.C.; writing—original draft preparation, S.P.; writing—review and editing, S.P., A.C. and B.L. All authors have read and agreed to the published version of the manuscript.	319
Funding: This study was supported by the National Institute on Aging of the National Institutes of Health under award number K25AG070286.	320
Institutional Review Board Statement: “The study was conducted in accordance with the Declaration of Helsinki, and approved by the Institutional Review Board (or Ethics Committee) of Johns Hopkins University.	321
Informed Consent Statement: Informed consent was obtained from all subjects involved in the study.	322
Data Availability Statement: The datasets presented in this article are not readily available because the datasets consist of clinical images of patients with rosacea. The source code for the FACES classification algorithm is available in the supplementary data.	323
Conflicts of Interest: The authors declare no conflict of interest.	324
References	325
1. Buddenkotte, J.; Steinhoff, M. Recent Advances in Understanding and Managing Rosacea. <i>F1000Research</i> 2018 , doi:10.12688/f1000research.16537.1.	326
2. Two, A.M.; Wu, W.; Gallo, R.L.; Hata, T.R. Rosacea: Part I. Introduction, Categorization, Histology, Pathogenesis, and Risk Factors. <i>J. Am. Acad. Dermatol.</i> 2015 .	327
3. Rainer, B.M.; Kang, S.; Chien, A.L. Rosacea: Epidemiology, Pathogenesis, and Treatment. <i>Dermatoendocrinol.</i> 2017 , doi:10.1080/19381980.2017.1361574.	328
4. Li, J.; Wang, B.; Deng, Y.; Shi, W.; Jian, D.; Liu, F.; Huang, Y.; Tang, Y.; Zhao, Z.; Huang, X.; et al. Epidemiological Features of Rosacea in Changsha, China: A Population-Based, Cross-Sectional Study. <i>J. Dermatol.</i> 2020 , doi:10.1111/1346-8138.15301.	329
5. Odom, R. The Nosology of Rosacea. <i>Cutis</i> 2004 .	330
6. Wilkin, J.; Dahl, M.; Detmar, M.; Drake, L.; Feinstein, A.; Odom, R.; Powell, F. Standard Classification of Rosacea: Report of the National Rosacea Society Expert Committee on the Classification and Staging of Rosacea. <i>J. Am. Acad. Dermatol.</i> 2002 , doi:10.1067/mjd.2002.120625.	331
7. Zhao, Z.; Wu, C.M.; Zhang, S.; He, F.; Liu, F.; Wang, B.; Huang, Y.; Shi, W.; Jian, D.; Xie, H.; et al. A Novel Convolutional Neural Network for the Diagnosis and Classification of Rosacea: Usability Study. <i>JMIR Med. Informatics</i> 2021 , doi:10.2196/23415.	332
8. Goceri, E.; Gunay, M. Automated Detection of Facial Disorders (ADFD): A Novel Approach Based-on Digital Photographs. <i>Comput. Methods Biomed. Eng. Imaging Vis.</i> 2018 , doi:10.1080/21681163.2017.1317292.	333
9. Gallo, R.L.; Granstein, R.D.; Kang, S.; Mannis, M.; Steinhoff, M.; Tan, J.; Thiboutot, D. Standard Classification and Pathophysiology of Rosacea: The 2017 Update by the National Rosacea Society Expert Committee. <i>J. Am. Acad. Dermatol.</i> 2018 .	334
10. Wang, Y.A.; James, W.D. Update on Rosacea Classification and Its Controversies. <i>Cutis</i> 2019 .	335
11. Zhou, M.; Xie, H.; Cheng, L.; Li, J. Clinical Characteristics and Epidermal Barrier Function of Papulopustular Rosacea: A Comparison Study with Acne Vulgaris. <i>Pakistan J. Med. Sci.</i> 2016 , doi:10.12669/pjms.326.11236.	336
12. Kadampur, M.A.; Al Riyae, S. Skin Cancer Detection: Applying a Deep Learning Based Model Driven Architecture in the	337

- Cloud for Classifying Dermal Cell Images. *Informatics Med. Unlocked* **2020**, doi:10.1016/j.imu.2019.100282. 360
13. Tozour, J.N.; Bandremer, S.; Patberg, E.; Zavala, J.; Akerman, M.; Chavez, M.; Mann, D.M.; Testa, P.A.; Vintzileos, A.M.; Heo, H.J. Application of Telemedicine Video Visits in a Maternal-Fetal Medicine Practice at the Epicenter of the COVID-19 Pandemic. *Am. J. Obstet. Gynecol. MFM* **2021**, doi:10.1016/j.ajogmf.2021.100469. 361
362
363
14. Binol, H.; Plotner, A.; Sopkovich, J.; Kaffenberger, B.; Niazi, M.K.K.; Gurcan, M.N. Ros-NET: A Deep Convolutional Neural Network for Automatic Identification of Rosacea Lesions. *Ski. Res. Technol.* **2020**, doi:10.1111/srt.12817. 364
365
15. Thomsen, K.; Christensen, A.L.; Iversen, L.; Lomholt, H.B.; Winther, O. Deep Learning for Diagnostic Binary Classification of Multiple-Lesion Skin Diseases. *Front. Med.* **2020**, doi:10.3389/fmed.2020.574329. 366
367
16. Jojoa Acosta, M.F.; Caballero Tovar, L.Y.; Garcia-Zapirain, M.B.; Percybrooks, W.S. Melanoma Diagnosis Using Deep Learning Techniques on Dermatoscopic Images. *BMC Med. Imaging* **2021**, doi:10.1186/s12880-020-00534-8. 368
369
17. Brinker, T.J.; Hekler, A.; Utikal, J.S.; Grabe, N.; Schadendorf, D.; Klode, J.; Berking, C.; Steeb, T.; Enk, A.H.; Von Kalle, C. Skin Cancer Classification Using Convolutional Neural Networks: Systematic Review. *J. Med. Internet Res.* **2018**. 370
371
18. Phillips, M.; Marsden, H.; Jaffe, W.; Matin, R.N.; Wali, G.N.; Greenhalgh, J.; McGrath, E.; James, R.; Ladoyanni, E.; Bewley, A.; et al. Assessment of Accuracy of an Artificial Intelligence Algorithm to Detect Melanoma in Images of Skin Lesions. *JAMA Netw. Open* **2019**, doi:10.1001/jamanetworkopen.2019.13436. 372
373
374
19. Brinker, T.J.; Hekler, A.; Hauschild, A.; Berking, C.; Schilling, B.; Enk, A.H.; Haferkamp, S.; Karoglan, A.; von Kalle, C.; Weichenthal, M.; et al. Comparing Artificial Intelligence Algorithms to 157 German Dermatologists: The Melanoma Classification Benchmark. *Eur. J. Cancer* **2019**, doi:10.1016/j.ejca.2018.12.016. 375
376
377
20. Aractingi, S.; Pellacani, G. Computational Neural Network in Melanocytic Lesions Diagnosis: Artificial Intelligence to Improve Diagnosis in Dermatology? *Eur. J. Dermatology* **2019**. 378
379
21. Fujisawa, Y.; Otomo, Y.; Ogata, Y.; Nakamura, Y.; Fujita, R.; Ishitsuka, Y.; Watanabe, R.; Okiyama, N.; Ohara, K.; Fujimoto, M. Deep-Learning-Based, Computer-Aided Classifier Developed with a Small Dataset of Clinical Images Surpasses Board-Certified Dermatologists in Skin Tumour Diagnosis. *Br. J. Dermatol.* **2019**, doi:10.1111/bjd.16924. 380
381
382
22. Esteva, A.; Kuprel, B.; Novoa, R.A.; Ko, J.; Swetter, S.M.; Blau, H.M.; Thrun, S. Dermatologist-Level Classification of Skin Cancer with Deep Neural Networks. *Nature* **2017**, doi:10.1038/nature21056. 383
384
23. Hosny, K.M.; Kassem, M.A.; Foad, M.M. Skin Cancer Classification Using Deep Learning and Transfer Learning. In Proceedings of the 2018 9th Cairo International Biomedical Engineering Conference, CIBEC 2018 - Proceedings; 2019. 385
386
24. El-Khatib, H.; Popescu, D.; Ichim, L. Deep Learning-Based Methods for Automatic Diagnosis of Skin Lesions. *Sensors (Switzerland)* **2020**, doi:10.3390/s20061753. 387
388
25. Codella, N.; Cai, J.; Abedini, M.; Garnavi, R.; Halpern, A.; Smith, J.R. Deep Learning, Sparse Coding, and SVM for Melanoma Recognition in Dermoscopy Images. In Proceedings of the Lecture Notes in Computer Science (including subseries Lecture Notes in Artificial Intelligence and Lecture Notes in Bioinformatics); 2015. 389
390
391
26. Goceri, E. Skin Disease Diagnosis from Photographs Using Deep Learning. In *Lecture Notes in Computational Vision and Biomechanics*; 2019. 392
393
27. Thomsen, K.; Iversen, L.; Titlestad, T.L.; Winther, O. Systematic Review of Machine Learning for Diagnosis and Prognosis in Dermatology. *J. Dermatolog. Treat.* **2020**. 394
395
28. Ramli, R.; Malik, A.S.; Hani, A.F.M.; Yap, F.B. Bin Segmentation of Acne Vulgaris Lesions. In Proceedings of the Proceedings - 2011 International Conference on Digital Image Computing: Techniques and Applications, DICTA 2011; 2011. 396
397
29. Aggarwal, L.P. Data Augmentation in Dermatology Image Recognition Using Machine Learning. *Ski. Res. Technol.* **2019**, doi:10.1111/srt.12726. 398
399
30. Binol, H.; Niazi, M.K.K.; Plotner, A.; Sopkovich, J.; Kaffenberger, B.; Gurcan, M.N. A Multidimensional Scaling and Sample Clustering to Obtain a Representative Subset of Training Data for Transfer Learning-Based Rosacea Lesion Identification.; 400
401

2020.	402
31. Goceri, E. Deep Learning Based Classification of Facial Dermatological Disorders. <i>Comput. Biol. Med.</i> 2021 , doi:10.1016/j.combiomed.2020.104118.	403
32. Seeland, M.; Mäder, P. Multi-View Classification with Convolutional Neural Networks. <i>PLoS One</i> 2021.	405
33. Guarino, A.; Malandrino, D.; Zaccagnino, R. An Automatic Mechanism to Provide Privacy Awareness and Control over Unwittingly Dissemination of Online Private Information. <i>Comput. Networks</i> 2022 , doi:10.1016/j.comnet.2021.108614.	406
34. He, K.; Zhang, X.; Ren, S.; Sun, J. Deep Residual Learning for Image Recognition. In Proceedings of the Proceedings of the IEEE Computer Society Conference on Computer Vision and Pattern Recognition; 2016.	408
35. Elgendi, M.; Nasir, M.U.; Tang, Q.; Fletcher, R.R.; Howard, N.; Menon, C.; Ward, R.; Parker, W.; Nicolaou, S. The Performance of Deep Neural Networks in Differentiating Chest X-Rays of COVID-19 Patients From Other Bacterial and Viral Pneumonias. <i>Front. Med.</i> 2020 , doi:10.3389/fmed.2020.00550.	411
36. Pathak, D.; Raju, U.S.N. Content-Based Image Retrieval Using Group Normalized-Inception-Darknet-53. <i>Int. J. Multimed. Inf. Retr.</i> 2021 , doi:10.1007/s13735-021-00215-4.	413
37. Wen, L.; Li, X.; Gao, L. A Transfer Convolutional Neural Network for Fault Diagnosis Based on ResNet-50. <i>Neural Comput. Appl.</i> 2020 , doi:10.1007/s00521-019-04097-w.	415
38. Szegedy, C.; Liu, W.; Jia, Y.; Sermanet, P.; Reed, S.; Anguelov, D.; Erhan, D.; Vanhoucke, V.; Rabinovich, A. Going Deeper with Convolutions. In Proceedings of the Proceedings of the IEEE Computer Society Conference on Computer Vision and Pattern Recognition; 2015.	417
39. Ma, N.; Zhang, X.; Zheng, H.T.; Sun, J. Shufflenet V2: Practical Guidelines for Efficient Cnn Architecture Design. In Proceedings of the Lecture Notes in Computer Science (including subseries Lecture Notes in Artificial Intelligence and Lecture Notes in Bioinformatics); 2018.	420
40. Hilbring, C.; Augustin, M.; Kirsten, N.; Mohr, N. Epidemiology of Rosacea in a Population-Based Study of 161,269 German Employees. <i>Int. J. Dermatol.</i> 2022 , doi:10.1111/ijd.15989.	423
41. Chosidow, O.; Cribier, B. Epidemiology of Rosacea: Updated Data. In Proceedings of the Annales de Dermatologie et de Venereologie; 2011.	426
42. Al-Dabagh, A.; Davis, S.A.; McMichael, A.J.; Feldman, S.R. Rosacea in Skin of Color: Not a Rare Diagnosis. <i>Dermatol. Online J.</i> 2014 .	428
	429